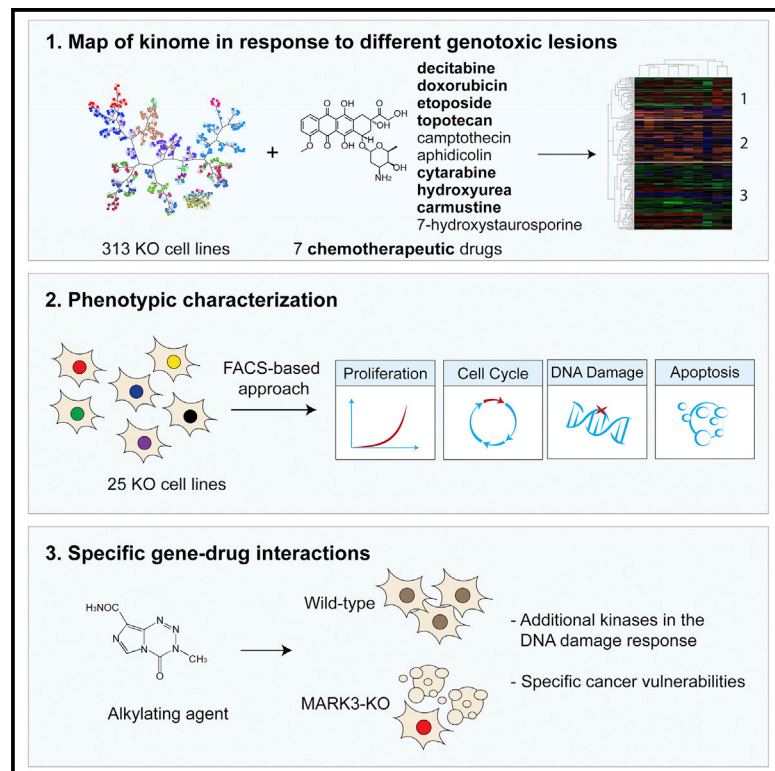


Cell Reports

Mapping the Human Kinome in Response to DNA Damage

Graphical Abstract



Authors

Michel Owusu, Peter Bannauer, Joana Ferreira da Silva, ..., Stefan Kubicek, Francesca D. Ciccarelli, Joanna I. Loizou

Correspondence

jloizou@cemm.oeaw.ac.at

In Brief

Cancer cells re-wire cellular networks, including those orchestrated by kinases. To identify therapeutic options for such cancers, Owusu et al. generated cell lines lacking kinases. They tested how these cell lines respond to DNA-damaging chemotherapeutics to identify sensitivity and resistance that can be exploited for cancer therapies.

Highlights

- Catalog of the human kinome in response to different types of genotoxic stress
- Synthetic vulnerability or resistance for kinases and DNA-damaging chemotherapeutics
- Identification of MARK3 as a kinase in the DNA damage response



Mapping the Human Kinome in Response to DNA Damage

Michel Owusu,¹ Peter Bannauer,¹ Joana Ferreira da Silva,¹ Thanos P. Mourikis,^{2,3} Alistair Jones,^{2,3} Peter Májek,¹ Michael Caldera,¹ Marc Wiedner,¹ Charles-Hugues Lardeau,^{1,3} André C. Mueller,¹ Jörg Menche,¹ Stefan Kubicek,^{1,4} Francesca D. Ciccarelli,^{2,3} and Joanna I. Loizou^{1,5,*}

¹CeMM Research Center for Molecular Medicine of the Austrian Academy of Sciences, Lazarettgasse 14, AKH BT 25.3, 1090 Vienna, Austria

²Cancer Systems Biology Laboratory, The Francis Crick Institute, London NW1 1AT, UK

³School of Cancer and Pharmaceutical Sciences, King's College London, London SE1 1UL, UK

⁴Christian Doppler Laboratory for Chemical Epigenetics and Antiinfectives, CeMM Research Center for Molecular Medicine of the Austrian Academy of Sciences, 1090 Vienna, Austria

⁵Lead Contact

*Correspondence: jloizou@cemm.oeaw.ac.at

<https://doi.org/10.1016/j.celrep.2018.12.087>

SUMMARY

We provide a catalog for the effects of the human kinome on cell survival in response to DNA-damaging agents, covering all major DNA repair pathways. By treating 313 kinase-deficient cell lines with ten diverse DNA-damaging agents, including seven commonly used chemotherapeutics, we identified examples of vulnerability and resistance that are kinase specific. To investigate synthetic lethal interactions, we tested the response to carmustine for 25 cell lines by establishing a phenotypic fluorescence-activated cell sorting (FACS) assay designed to validate gene-drug interactions. We show apoptosis, cell cycle changes, and DNA damage and proliferation after alkylation- or crosslink-induced damage. In addition, we reconstitute the cellular sensitivity of *DYRK4*, *EPHB6*, *MARK3*, and *PNCK* as a proof of principle for our study. Furthermore, using global phosphoproteomics on cells lacking *MARK3*, we provide evidence for its role in the DNA damage response. Our data suggest that cancers with inactivating mutations in kinases, including *MARK3*, are particularly vulnerable to alkylating chemotherapeutic agents.

INTRODUCTION

The DNA damage response (DDR) is elicited by a complex and far-reaching network of proteins that are commonly deregulated in human pathologies, including cancer (Jackson and Bartek, 2009). Besides surgery, the most common treatment for cancer patients is radio- or chemotherapy. To date, some of the commonly used chemotherapeutic compounds are DNA-damaging agents (Helleday et al., 2008). Such agents can cause cell death by targeting either DNA directly or proteins implicated in DNA repair and replication, cell cycle regulators, or signal transducers. Protein kinases are an important group of signal transducers and are often deregulated in human cancer (Fleuren et al., 2016), making them particularly interesting to study within

the signaling context of the DNA damage response. Moreover, due to their enzymatic function, kinases represent an important group of drug targets (Klaeger et al., 2017) and therefore, results from loss-of-function studies with kinases are more likely to be translated into a therapeutic setting.

Kinases have broad functions following DNA damage. For instance, the ATM superfamily, which includes ATM, ATR, and DNA-PKcs (encoded by the gene *PRKDC*), is involved in sensing or amplifying initial signals of DNA lesions (Hiom, 2005; Maréchal and Zou, 2013). CHK1 and CHK2 kinases regulate cell cycle progression in response to DNA damage, providing time for DNA repair (Lazzaro et al., 2009; Manic et al., 2015). Other kinases, such as ABL1, are involved in transducing or fine-tuning signals resulting from DNA damage, which can ultimately lead to survival, senescence, or cell death (Kharbanda et al., 1998). Though some kinases have been studied in depth, the role of many is still not known (Fedorov et al., 2010).

Here, we used CRISPR-Cas9 to individually delete expressed and non-essential kinases in human HAP1 cells. Next, we performed a drug screen using DNA-damaging agents, selected to cover all major DNA repair pathways, to map drug-specific sensitivities and resistances. We validated selected drug-gene interactions in response to alkylation-induced damage and assessed the contribution of apoptosis, DNA damage, cell cycle arrest, and proliferation, leading to cellular sensitivities or resistances by designing and utilizing a phenotypic assay. In addition, we performed global phosphoproteomics to reveal alterations in phospho-signaling in the absence of *MARK3*, a kinase that is frequently mutated in cancer and we identified as displaying a vulnerability to alkylation damage, hence showing a role for *MARK3* in the DNA damage response.

RESULTS

We used CRISPR-Cas9 to target 313 expressed and non-essential kinases in human HAP1 cells and produce clonal knockout cell lines (Blomen et al., 2015; Table S1). The kinases targeted cover all groups according to the standard classification scheme of kinases (Manning et al., 2002), hence ensuring coverage of the family (Figure 1A). To examine the response of the non-essential human kinome to a broad range of DNA-damaging agents, we



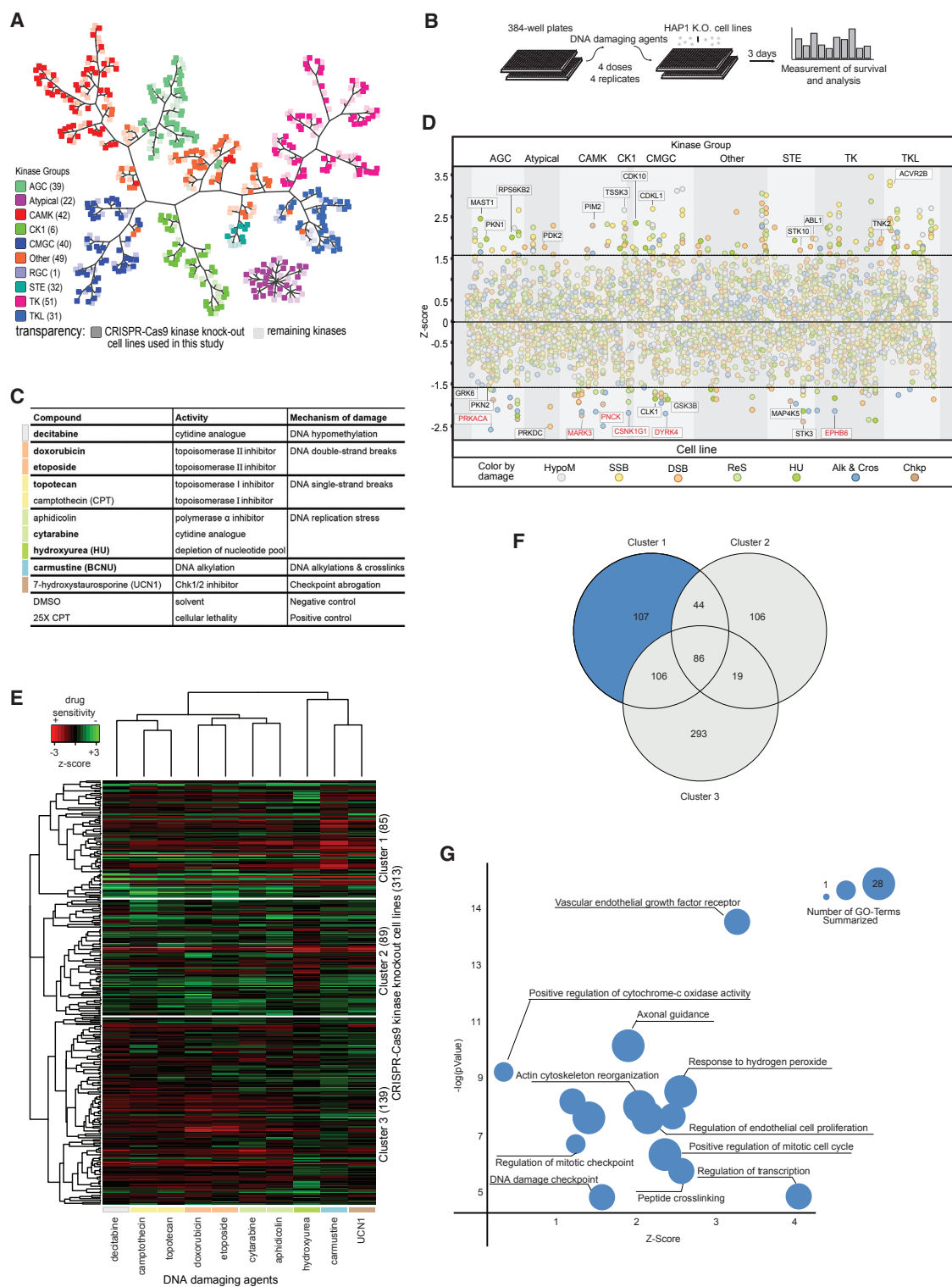


Figure 1. Survival of Non-essential Kinome in Response to DNA Damage

(A) Kinome tree representing all kinases (Manning et al., 2002). In bold squares are the kinases targeted by CRISPR-Cas9 (313) and in light squares are the remaining kinases.

(B) Workflow of survival assay. Dose responses were performed with 4 concentrations in 4 replicates. Cells were incubated with compounds for 3 days, and survival was performed using a luminescent readout.

(legend continued on next page)

first designed and optimized our approach using DNA-repair-deficient cell lines, where we were able to recover known gene-drug interactions (Figures 1B, S1A, and S1B). Based on this approach, we selected 10 compounds that induce different types of DNA damage and thus utilize distinct DNA repair pathways which are frequently used as chemotherapeutics (Figure 1C). Next, we exposed the 313 kinase-deficient cell lines to these compounds at four concentrations and assessed cellular survival after three days (Figure 1B).

In line with the literature, most cell lines showing strong sensitivity or resistance to the selected compounds were anticipated (Figure 1D; Table S1). For instance, PRKDC-deficient cells showed the strongest sensitivity to the DNA double-strand-break-inducing agents, etoposide and doxorubicin, whereas ABL1-deficient cells showed resistance to those agents (Kharbanda et al., 1998). A clustering of the cell lines by their sensitivity to the 10 compounds revealed 3 clusters, characterized by high sensitivity to carmustine (cluster 1), hydroxyurea (cluster 2), and DNA double-strand-break-inducing agents, such as etoposide and doxorubicin (cluster 3; Figure 1E; Table S1). We found that compounds with similar modes of action were closer in the clustering, as illustrated by topoisomerase II inhibitors (doxorubicin and etoposide), topoisomerase I inhibitors (topotecan and camptothecin), and agents that induced replicative stress (aphidicolin and cytarabine). Due to their clustering with DNA double-strand-break-inducing agents, our data support the notion that DNA double-strand breaks, following replication fork stalling and collapse, are one of the primary sources of cellular death after treatment with lethal concentrations of aphidicolin, cytarabine, or topoisomerase I inhibitors (Lin et al., 2009; Figure 1E). Cluster 1 was enriched for kinases that are particularly vulnerable to the alkylating agent carmustine, which indicates a synthetic lethality between those kinases and carmustine. Differential Gene Ontology (GO) term enrichment analysis confirmed that cluster 1 was uniquely enriched for terms previously associated with the cellular response to alkylating or crosslinking agents, including the upregulation of vascular endothelial growth factor receptors (Cheppudira et al., 2008) and induction of oxidative stress (Helal and Helal, 2009; cellular response to hydrogen peroxide; positive regulation of cytochrome-c oxidase activity), which in turn leads to actin cytoskel-

eton reorganization (Pujol-Carrion and de la Torre-Ruiz, 2010; Figures 1F and 1G; Table S1). Cluster 2 was enriched for kinases that are synthetic lethal with hydroxyurea. GO term enrichment analysis revealed their association with terms such as apoptosis or cell adhesion (Figure S1C; Table S1), supporting previous findings (Bartolucci et al., 2010).

Because kinases are highly associated with cancer (Torkamani et al., 2009), and as enzymes, are potentially amenable to chemical inhibition, we focused on carmustine-dependent synthetic lethal interactions. Moreover, we found that cell lines lacking MARK3, PRKACA, CSNK1G1, PNCK, DYRK4, or EPHB6 in combination with carmustine showed the strongest unreported synthetic lethal interactions (Figure 1D). To validate and further dissect the mechanism of cellular sensitivity to the drug, we measured DNA damage, apoptosis, cell cycle phases, and proliferation in those cell lines in a fluorescence-activated cell sorting (FACS)-based phenotypic assay (Figure 2A) with the markers γ H2AX, TUNEL, DAPI, and EdU, respectively. As controls, we included the following cell lines lacking proteins previously linked to the signaling of DNA damage or DNA repair: PRKDC (Shrivastav et al., 2008); ABL1 (Shafman et al., 1997); PDK2 (Vinięgra et al., 2005); PIM2 (Zirkin et al., 2013); and TNK2 (Mahajan et al., 2012). We also included the cell cycle proteins CDK10, CLK1, and CDKL1 (Malumbres, 2014); the cell death proteins GRK6 (Le et al., 2016; Xu et al., 2017), GSK3B (Grassilli et al., 2013), MAST1 (De Angelis et al., 2006), STK10 (Fukumura et al., 2013), and STK3 (Lee et al., 2001); as well as TSSK3, a protein whose loss correlates with a strong general resistance to DNA-damaging agents, as revealed in our study (Figure 1D).

Carmustine is a chemotherapeutic agent used for the treatment of several types of cancer, particularly those relating to the nervous system, such as glioblastoma (Affronti et al., 2009; Chaichana et al., 2011). It is a bifunctional alkylating agent that produces DNA mono-alkylation adducts as well as DNA intra- and interstrand crosslinks (ICLs) (Kondo et al., 2010; Nikolova et al., 2017). Almost all of the lesions (90%–95%) produced by bifunctional alkylating agents are mono-alkylation adducts (Muniandy et al., 2010), such as N⁷-methylguanine or O⁶-methylguanine. However, the less abundant (ca. 5%) DNA crosslinks, particularly ICLs, form the most deleterious lesions (Muniandy et al., 2010) and can interfere

(C) List of the 10 DNA-damaging compounds selected for use in the survival assay. Compounds with similar modes of action share the same color label.

(D) Survival response of cell lines to compounds with kinases from the same kinase groups clustered together in columns. Each vertical line represents a particular knockout cell line with all of its gene-drug interactions. Compounds are depicted as different color-coded bubbles. HypoM (hypomethylating agent; decitabine), SSB (single-strand-break-inducing agents), DSB (double-strand-break-inducing agents), ReS (replication-stress-inducing agents), HU (replication-stress-inducing agent hydroxyurea), Alk and Cros (alkylating and crosslinking agent; BNCU), and Chkp (Chk1 inhibitor) are shown. Z scores were calculated for the area under the curve (AUC) of 4 concentrations across the mean of 4 replicates for each cell line. Lines are set at Z scores greater than 1.65 or less than -1.65 ($p < 0.05$). The names of some expected or known interactions are labeled in black font. Names in red font are examples of lethal interactions after carmustine treatment. AGC, protein kinase families A, G and C; CAMK, calmodulin/calcium-regulated kinases; CK1, casein kinase 1; CMGC, CDK, MAPK, GSK3, CLK family; RGC, receptor guanylate cyclases; STE, STE7, STE11, and STE20 homologs; TK, tyrosine kinase; TKL, tyrosine kinase like.

(E) Clustering of 313 kinase-deficient cell lines in response to diverse DNA-damaging agents reveals three distinct clusters (left dendrogram): cluster 1 is characterized by a sensitivity to carmustine; cluster 2 by a sensitivity to hydroxyurea; and cluster 3 by a sensitivity to DNA double-strand-break-inducing agents, notably etoposide and doxorubicin. Compounds with similar modes of action (color labels) are closer in neighborhood (top dendrogram): topoisomerase II inhibitors (doxorubicin and etoposide); topoisomerase I inhibitors (topotecan and camptothecin); and replication-stress-inducing agents by fork stalling (cytarabine and aphidicolin).

(F) Gene Ontology (GO) term enrichment analysis for clusters 1–3.

(G) GO terms enriched for cluster 1 uniquely.

See also Figure S1 and Table S1.

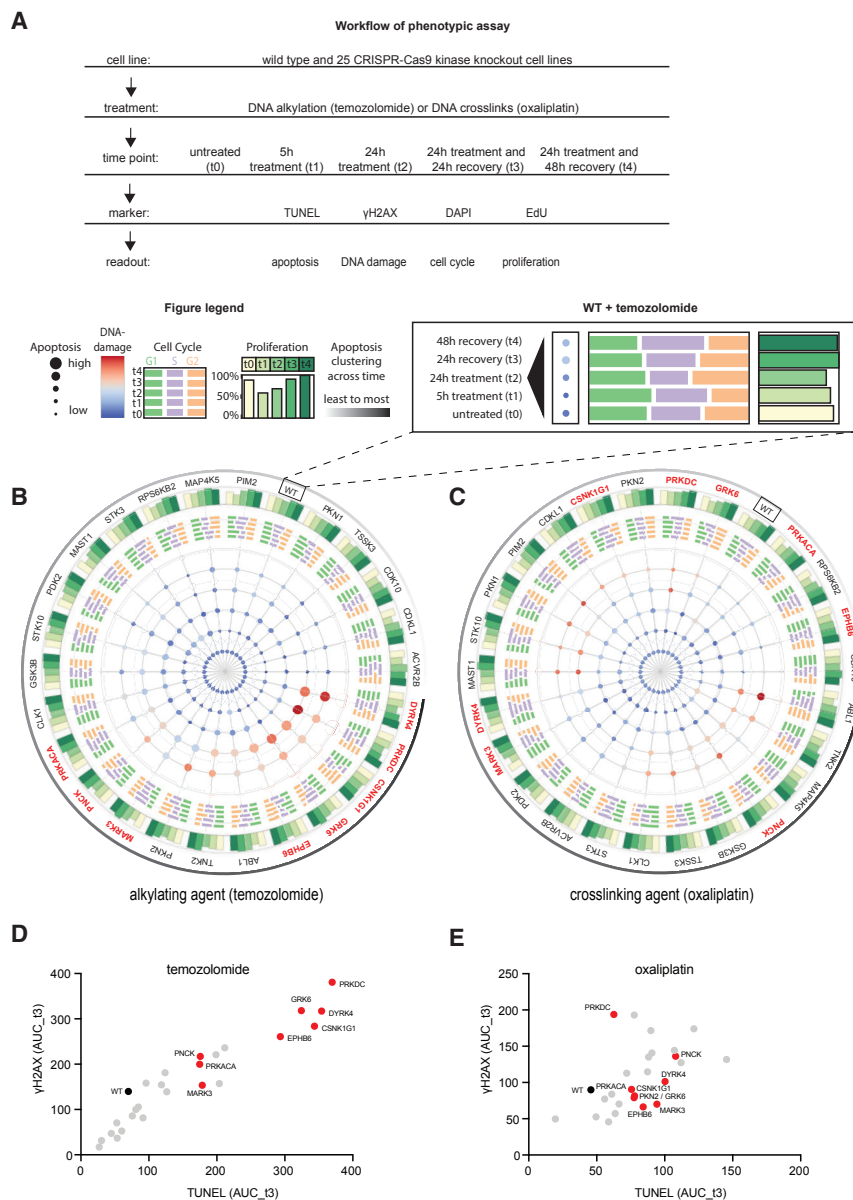


Figure 2. Phenotypic Validation of Cellular Sensitivity to Alkylating Agents

(A) Workflow of phenotypic screen. Wild-type and 25 CRISPR-Cas9 knockout cell lines were treated with alkylating or crosslinking agents (temozolomide or oxaliplatin, respectively) for 5 or 24 h, after which drug medium was replaced with fresh medium to allow cells to recover from damage. EdU incorporation was performed for 40 min before harvest. Cells were fixed and co-stained using the following markers: TUNEL for apoptosis; anti- γ H2AX for DNA damage; DAPI for cell cycle; and EdU stain for proliferation. Cells were analyzed by flow cytometry. For each stain, the six concentrations for each time point were summarized with an AUC calculation. (Bottom) Figure legend and phenotypic plot of wild-type HAP1 cells after temozolomide treatment (right) are shown.

(B and C) Phenotypic plot for cell lines after alkylation-induced damage by temozolomide (B) or crosslinking-induced damage by oxaliplatin (C). The inner-most circle of the phenotypic plot shows DNA damage (color gradient of bubbles) and apoptosis (size of bubbles) for 4 different time points, t1–t4, from center to periphery, and indicated cell lines. The next circle (middle) shows cell cycle distribution of cell lines in G1 (green), S (purple), and G2/M (orange) for time points t1–t4, from center to periphery. The outermost circle shows proliferation changes of cell lines at time point t1–t4. Cell lines are ordered hierarchically according to apoptosis, and names are indicated outside of the phenotypic plot. Knockouts identified to be sensitive to carmustine (red names) show a high level of apoptosis to temozolomide (7/10), but not to oxaliplatin (2/10), indicating that the survival response is primarily due to alkylating and not crosslinking lesions. Wild-type HAP1 cells (WT) are highlighted in a box. Figure legend is as in (A). (D and E) Depiction of γ H2AX and TUNEL signals for time point t3 following exposure to (D) temozolomide and (E) oxaliplatin. See also Figure S2 and Table S2.

with replication or transcription and trigger apoptosis and cell cycle arrest (Nikolova et al., 2017). In order to confirm that the predominant cause of cellular toxicity to carmustine was due to the effects of alkylation, we used the monofunctional alkylating agent temozolomide (TMZ), which does not produce crosslinks and is often used as a superior replacement therapy to carmustine (Vinjamuri et al., 2009), as well as the crosslinking agent oxaliplatin (Figure S1B). We chose concentrations of the compounds that moderately affect wild-type cells and, as expected, both compounds induced apoptosis, DNA damage, G2/M cell cycle arrest, and a reduction of proliferating cells in a dose- and time-dependent manner (Hirose et al., 2001; William-Faltaos et al., 2007; Figures 2B and 2C). Hierarchical clustering of the cell lines according to apoptosis confirmed that the

most sensitive survival interactions after carmustine (Figure 1D) showed the highest apoptosis after TMZ in the phenotypic assay (Figures 2D, 2E, S2A, and S2B; Table S2).

DNA damage as measured by γ H2AX can either be a cause or consequence of apoptosis (Rogakou et al., 2000). For a gene to be involved in the signaling or repair of DNA damage, we would expect to see higher levels of γ H2AX preceding or coinciding with higher levels of apoptosis. For instance, DYRK4-deficient cells showed a peak of apoptosis 24 h after treatment followed by a peak of γ H2AX at 48 h of treatment (Figure 2B). Hence, the γ H2AX signal at the 48 h time point may therefore be a consequence of apoptosis in DYRK4-deficient cells. This may also be the case for PNCK and PKN2 (Figure 2B). In contrast, PRKDC-deficient cells, which have a deficiency in DNA repair, showed the maximum levels of γ H2AX and apoptosis early, at

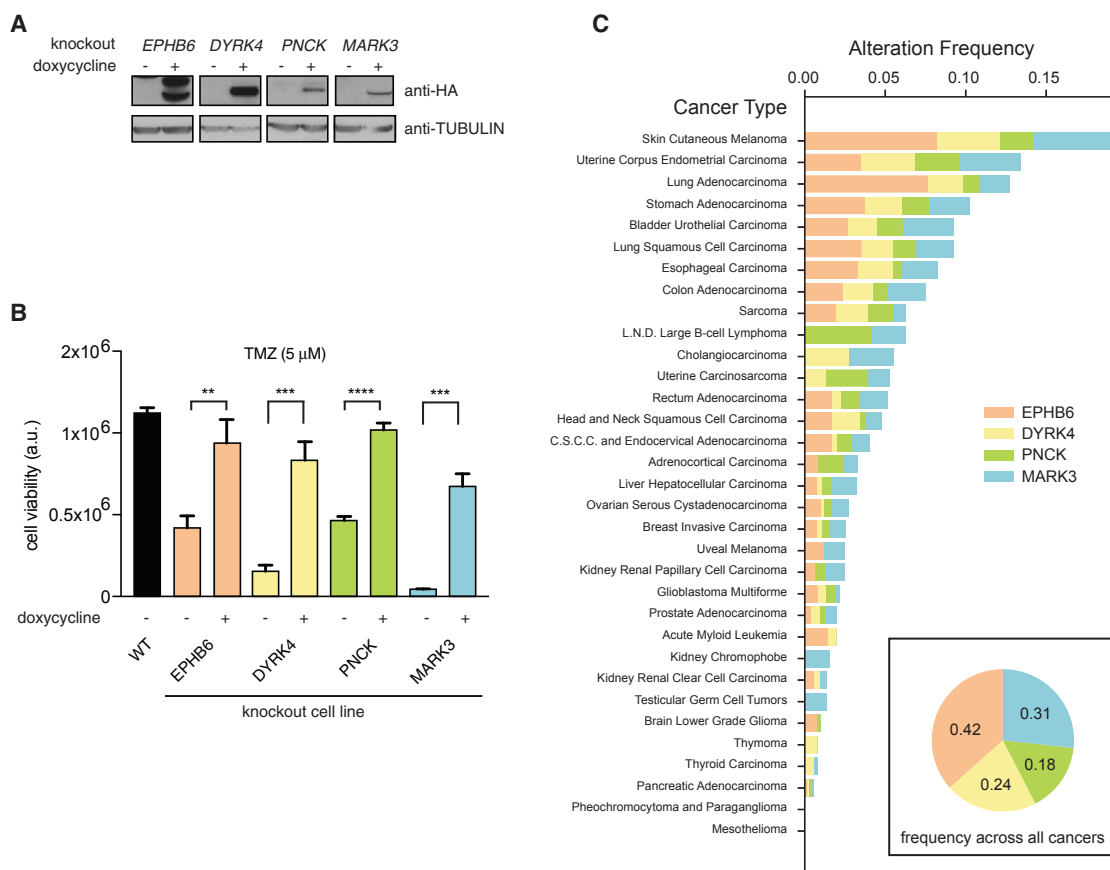


Figure 3. Genetic Validation and Cancer Association of DYRK4, EPHB6, PNCK, or MARK3

(A and B) Rescue of sensitivity to alkylating agents after reconstitution of knockout cell lines with HA-tagged, doxycycline-inducible DYRK4, EPHB6, PNCK, or MARK3 proteins.

(A) Anti-HA immunoblot of the indicated cells lines reconstituted with the relevant cDNA after doxycycline induction. EPHB6 shows a characteristic smear of a fragmented membrane protein by immunoblotting. “*” indicates non-specific band. Tubulin was used as a loading control.

(B) Survival of DYRK4-, EPHB6-, PNCK-, and MARK3-deficient cells after reconstitution of exogenous proteins by doxycycline induction following temozolomide (TMZ) treatment. Results are means of 3 replicates with SDs.

(C) Loss-of-function mutations (missense and non-sense mutations) of indicated genes in cancer. C.S.C.C., cervical squamous cell carcinoma; L.N.D., lymphoid neoplasm diffuse.

See also Figure S3.

24 h after treatment, followed by a slow but coinciding recovery of γ H2AX and apoptosis at 48 h after treatment (Figure 2B). A similar albeit weaker phenotype can be observed in cells deficient for CSNK1G1, EPHB6, MARK3, and PRKACA (Figure 2B). Interestingly, we also observed a strong and persistent G2/M arrest in cells deficient for CSNK1G1 or EPHB6 (Figure 2B). Although the sensitivity of these kinase-deficient cells to alkylating agents is as of yet unreported, it is in line with what is known about their function, as CSNK1G1 has previously been shown to regulate the kinase CHK1, which is a cell cycle regulator following DNA damage (Meng et al., 2011) whereas EPHB6 has been linked to the regulation of NPAT, a DNA-damage-signaling and cell cycle regulator (Kandpal, 2010).

After confirming selected cellular survival phenotypes in our phenotypic screen, we next sought to validate gene-drug interactions in knockout cell lines by reconstitution of the wild-type genes. We selected the less studied kinases, DYRK4, EPHB6,

PNCK, and MARK3, as well as control kinases with resistance phenotypes, ABL1 and TSSK3 (Figures S3A and S3B). After expression of hemagglutinin (HA)-tagged inducible proteins in the respective deficient cell lines, we assessed whether cellular survival to DNA damage was reverted (Figures 3A and 3B). Indeed, the sensitivity and resistance phenotypes could be corrected by recombinant expression of the relevant kinase, hence establishing a coherent genotype-phenotype relationship (Figures 3B and S3C–S3E). ABL1- and TSSK3-deficient cells, which showed resistance to doxorubicin or hydroxyurea in the survival screen, became significantly sensitive after reconstitution (Figures S3C–S3E), whereas DYRK4, EPHB6, PNCK, and MARK3, which showed resistance in survival after alkylation-induced damage, became significantly more resistant after reconstitution of the respective wild-type genes (Figure 3B). We observed no differences in the survival of wild-type cells after overexpression of DYRK4, EPHB6, PNCK, or MARK3 following treatment with

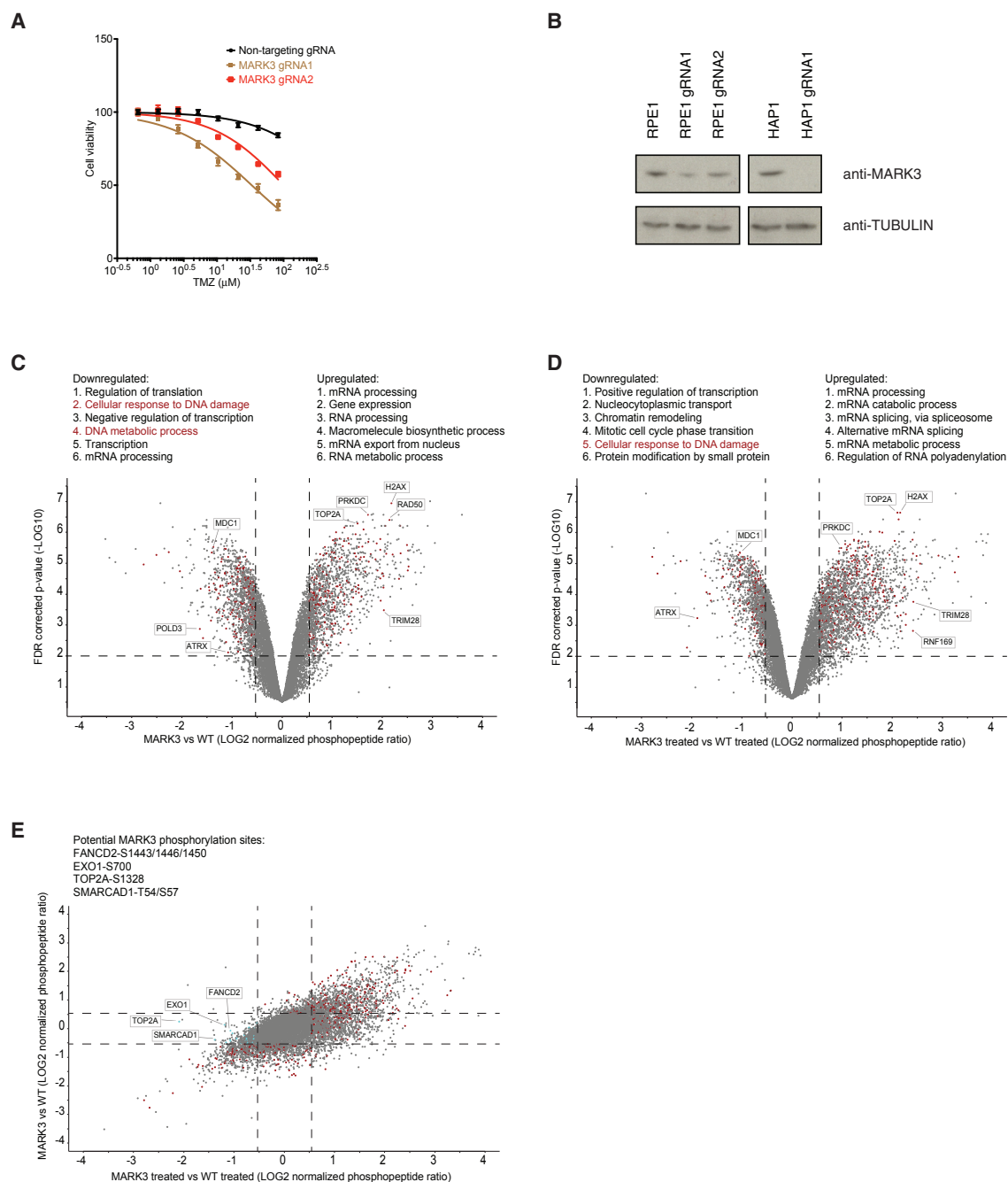


Figure 4. Characterization of MARK3 in Response to Alkylation Damage

(A) Survival of RPE1 cells expressing a non-targeting and two independent single guide RNAs (gRNAs) against MARK3. Cells were treated with the indicated TMZ concentrations for 3 days, following which survival was measured. Data represent 3 replicates with SDs.

(B) Immunoblot of MARK3 in RPE1 cells using two non-overlapping gRNAs (gRNA1 and 2). Tubulin was used as a loading control. The immunoblot was performed on a pooled population of RPE1 cells and corresponds to the cells used in the survival curve in (A). The HAP1 cells targeted with gRNA1 for MARK3 were derived from a clonal population.

(C and D) Ratios of phosphopeptide intensities normalized to protein abundance changes for MARK3 knockout compared to wild-type, without (C) or with (D) TMZ treatment at 62.5 μM for 24 h. LIMMA statistical model and Benjamini-Hochberg procedure (false discovery rate [FDR] correction) were used to calculate statistical significance of observed changes. Tandem mass tags (TMTs) ratios with Q values lower than 0.01 were considered as significant. Horizontal dashed line represents $-\log_{10}(0.01)$, the FDR cutoff. Vertical dashed lines represent $\pm \log_2(1.45)$, corresponding to the 5% quantile of the distribution of ratios observed among biological replicates within the same sample types. Ratios of phosphopeptide intensities were normalized to ratios of corresponding protein intensities.

(legend continued on next page)

TMZ, indicating that their upregulation is not sufficient to render cells resistant (Figures S3F and S3G).

In order to investigate the clinical significance of our findings, we used data from the public database The Cancer Genome Atlas (TCGA) to determine the frequency of DYRK4, EPHB6, PNCK, and MARK3 loss-of-function mutations in cancer (Figure 3C). From these genes, mutations within EPHB6 or MARK3 occurred frequently in cancer (42% or 31%, respectively). Because kinases act by phosphorylating specific target substrate proteins, we sought to investigate the changes in intracellular phosphorylation events after loss of one of the kinases identified as being frequently mutated in cancer. We chose to investigate MARK3, because EPHB6 lacks an active kinase domain (Gurniak and Berg, 1996). In order to determine whether the effect of MARK3 loss was a general or a cell-specific response, we investigated the cellular sensitivity to TMZ in an independent cell line (RPE1), using two non-overlapping guide RNAs (Figures 4A and 4B). The data support the hypothesis that reduced levels of MARK3 sensitizes cells to TMZ.

To identify potential substrates of MARK3, we took a global phosphoproteomics approach. Observed levels of detected phosphoserine, phosphothreonine, and phosphotyrosine were normalized to the overall abundances of the respective proteins to capture changes in phosphorylation levels rather than of protein expression levels (Figures S4A–S4D; Tables S3 and S4). Depletion of MARK3 in the absence of exogenous DNA damage displayed considerable changes in the basal phosphorylation status of proteins (Figure 4C). GO term enrichment analysis of significantly regulated phospho-sites revealed a major downregulation in phosphorylation of proteins involved in the cellular response to DNA damage, although some markers of DNA damage, including phosphorylated H2AX, were upregulated (Figure 4C), thus indicating a role of MARK3 in DNA damage response. In order to identify potential substrates of MARK3, which may contribute to the observed increase in sensitivity toward alkylating agents, we treated wild-type and MARK3-deficient cells with a low dose of TMZ for 24 h (corresponding to the treatment of t1 in Figures 2A and 2B). Almost no significant changes in phosphorylation were observed upon TMZ treatment in wild-type cells, and 293 significantly up- and down-regulated phospho-sites (on 225 proteins) were detected for MARK3-deficient cells (Figures S4E and S4F). Global phosphorylation changes between treated and untreated wild-type and MARK3-deficient cells were small (Figures 4C and 4D); however, some phosphorylation sites were specifically downregulated in MARK3-deficient cells after TMZ treatment (Figure 4E). We reasoned that those phosphorylation sites might play a role in the sensitivity of MARK3 knockout cells toward alkylation-induced DNA damage and therefore could represent potential direct targets of MARK3-mediated phospho-signaling. Specifically, the downregulation of phospho-sites of known DNA damage response proteins, including EXO1, FANCD2, TOP2A, and

SMARCAD1, suggest a role for MARK3 in response to DNA damage. However, the contribution of other MARK3-dependent (and DNA-damage-independent) intracellular signaling events to the sensitivity of MARK3 knockout cells to alkylating agents cannot be excluded.

DISCUSSION

Unperturbed signaling of DNA damage is essential in guarding the genome against cancer (Bartkova et al., 2006). At the same time, targeting the DNA damage response has proven to be a successful strategy in cancer therapy. In this study, we have shown the response of 313 cell lines, lacking kinases involved in different cellular signaling pathways, against 10 diverse DNA-damaging agents, including 7 commonly used chemotherapeutics. In doing so, we have identified unreported synthetic lethal and resistance gene-drug interactions. For selected cell lines, we further probe the synthetic lethality with carmustine by designing a phenotypic assay to investigate and validate gene-drug interactions in a broad manner. We show apoptosis, cell cycle, DNA damage, and proliferation after alkylation or crosslink-induced damage for those cell lines. Moreover, we rescue the survival phenotype of DYRK4, EPHB6, MARK3, and PNCK as a proof-of-principle for our study in reconstitution experiments. MARK3 has been reported to be involved in the regulation of cell polarity (Suzuki et al., 2004). In this study we provide phosphoproteomic data implicating a role for MARK3 in the DNA damage response. The use of TMZ is so far restricted to cancers of the CNS (Thomas et al., 2017). Our data indicate that in the presence of MARK3 deficiency, which occurs in some cancers, TMZ could be an effective treatment strategy.

STAR★METHODS

Detailed methods are provided in the online version of this paper and include the following:

- KEY RESOURCES TABLE
- CONTACT FOR REAGENT AND RESOURCE SHARING
- EXPERIMENTAL AND SUBJECT DETAILS
 - Cell Lines
- METHOD DETAILS
 - Confirmation of CRISPR-Cas9 Targeting by Sanger Sequencing
 - High-throughput Drug Screen
 - FACS Screen
 - Reconstitution of Knockout Cell Lines
 - Survival Dose Responses
 - Immunoblotting and Antibodies
 - Targeting of MARK3 by CRISPR-Cas9 in RPE1 cells
 - Phosphoproteomics

Representative phosphosites on DNA damage response (DDR) proteins are labeled or marked in red. The first six most relevant GO terms from significantly up or downregulated phosphorylation substrates (protein names) are listed.

(E) Ratios of untreated versus treated condition. Potential DDR-related MARK3 targets are marked in turquoise and labeled along with a list of corresponding phosphosites.

See also Figure S4 and Tables S3 and S4.

● **QUANTIFICATION AND STATISTICAL ANALYSIS**

- Analysis of high-throughput Drug Screen (Figures 1 and S1, Table S1)
- Clustering Analysis (Figure 1 and Table S1)
- GO Term Enrichment Analysis (Figures 1, 4, S1, and S4, Table S1)
- FACS Analysis (Figures 2 and S2, Table S2)
- Gene Alteration Frequencies (Figure 3)
- Analysis of Phosphoproteomics (Figures 4 and S4, Tables S3 and S4)

SUPPLEMENTAL INFORMATION

Supplemental Information includes four figures and five tables and can be found with this article online at <https://doi.org/10.1016/j.celrep.2018.12.087>.

ACKNOWLEDGMENTS

Research in the Kubicek lab is supported by the Austrian Federal Ministry of Science, Research and Economy and the National Foundation for Research, Technology, and Development. M.O., P.B., and J.F.d.S. were supported by FWF grant awarded to J.I.L. (29555 and 29763). We thank Claudia Doppler and Jana Stranka for experimental assistance. We also thank Markus Müller, Lydia Robinson, Georgia Velimezi, Abdelghani Mazouzi, and Doris Chen for input on the project and manuscript.

AUTHOR CONTRIBUTIONS

M.O., P.B., M.W., C.-H.L., and A.C.M. carried out the experimental work. M.O., P.B., J.F.d.S., T.P.M., A.J., M.C., and P.M. performed data analysis. Writing was by M.O. with J.I.L. The project was conceptualized by M.O. and J.I.L. Project administration was by S.K., J.M., F.D.C., and J.I.L. Funding acquisition was by S.K., F.D.C., J.M., and J.I.L. All authors reviewed and commented on the manuscript.

DECLARATION OF INTERESTS

The authors declare no competing interests.

Received: March 23, 2018

Revised: October 31, 2018

Accepted: December 18, 2018

Published: January 15, 2019

REFERENCES

Affronti, M.L., Heery, C.R., Herndon, J.E., 2nd, Rich, J.N., Reardon, D.A., Desjardins, A., Vredenburgh, J.J., Friedman, A.H., Bigner, D.D., and Friedman, H.S. (2009). Overall survival of newly diagnosed glioblastoma patients receiving carmustine wafers followed by radiation and concurrent temozolomide plus rotational multiagent chemotherapy. *Cancer* *115*, 3501–3511.

Altschul, S.F., Gish, W., Miller, W., Myers, E.W., and Lipman, D.J. (1990). Basic local alignment search tool. *J. Mol. Biol.* *215*, 403–410.

Bartkova, J., Rezaei, N., Liontos, M., Karakaidos, P., Kleitsas, D., Issaeva, N., Vassiliou, L.-V.F., Kolettas, E., Niforou, K., Zoumpourlis, V.C., et al. (2006). Oncogene-induced senescence is part of the tumorigenesis barrier imposed by DNA damage checkpoints. *Nature* *444*, 633–637.

Bartolucci, P., Chaar, V., Picot, J., Bachir, D., Habibi, A., Fauroux, C., Galactéros, F., Colin, Y., Le Van Kim, C., and El Nemer, W. (2010). Decreased sickle red blood cell adhesion to laminin by hydroxyurea is associated with inhibition of Lu/BCAM protein phosphorylation. *Blood* *116*, 2152–2159.

Benjamini, Y., and Hochberg, Y. (2018). Controlling the False Discovery Rate: A Practical and Powerful Approach to Multiple Testing. *Journal of the Royal Statistical Society. Series B (Methodological)* *57*, 289–300.

Blomen, V.A., Májek, P., Jae, L.T., Bigenzahn, J.W., Nieuwenhuis, J., Staring, J., Sacco, R., van Diemen, F.R., Olk, N., Stukalov, A., et al. (2015). Gene essentiality and synthetic lethality in haploid human cells. *Science* *350*, 1092–1096.

Cerami, E., Gao, J., Dogrusoz, U., Gross, B.E., Sumer, S.O., Aksoy, B.A., Jacobsen, A., Byrne, C.J., Heuer, M.L., Larsson, E., et al. (2012). The cBio cancer genomics portal: an open platform for exploring multidimensional cancer genomics data. *Cancer Discov* *2*, 401–404.

Chaichana, K.L., Zaidi, H., Pendleton, C., McGirt, M.J., Grossman, R., Weingart, J.D., Olivi, A., Quiñones-Hinojosa, A., and Brem, H. (2011). The efficacy of carmustine wafers for older patients with glioblastoma multiforme: prolonging survival. *Neurol. Res.* *33*, 759–764.

Chen, E.Y., Tan, C.M., Kou, Y., Duan, Q., Wang, Z., Meirelles, G.V., Clark, N.R., and Ma'ayan, A. (2013). Enrichr: interactive and collaborative HTML5 gene list enrichment analysis tool. *BMC Bioinformatics* *14*, 128.

Cheppudira, B.P., Girard, B.M., Malley, S.E., Schutz, K.C., May, V., and Vizzard, M.A. (2008). Upregulation of vascular endothelial growth factor isoform VEGF-164 and receptors (VEGFR-2, Npn-1, and Npn-2) in rats with cyclophosphamide-induced cystitis. *Am. J. Physiol. Renal Physiol.* *295*, F826–F836.

De Angelis, P.M., Svendsrud, D.H., Kravik, K.L., and Stokke, T. (2006). Cellular response to 5-fluorouracil (5-FU) in 5-FU-resistant colon cancer cell lines during treatment and recovery. *Mol. Cancer* *5*, 20.

Englinger, B., Lötsch, D., Pirker, C., Mohr, T., van Schoonhoven, S., Boidol, B., Lardeau, C.-H., Spitzwieser, M., Szabó, P., Heffeter, P., et al. (2016). Acquired nintedanib resistance in FGFR1-driven small cell lung cancer: role of endothelin-A receptor-activated ABCB1 expression. *Oncotarget* *7*, 50161–50179.

Fedorov, O., Müller, S., and Knapp, S. (2010). The (un)targeted cancer kinome. *Nat. Chem. Biol.* *6*, 166–169.

Fleuren, E.D.G., Zhang, L., Wu, J., and Daly, R.J. (2016). The kinome 'at large' in cancer. *Nat. Rev. Cancer* *16*, 83–98.

Fukumura, K., Yamashita, Y., Kawazu, M., Sai, E., Fujiwara, S., Nakamura, N., Takeuchi, K., Ando, M., Miyazono, K., Ueno, T., et al. (2013). STK10 missense mutations associated with anti-apoptotic function. *Oncol. Rep.* *30*, 1542–1548.

Gao, J., Aksoy, B.A., Dogrusoz, U., Dresdner, G., Gross, B., Sumer, S.O., Sun, Y., Jacobsen, A., Sinha, R., Larsson, E., et al. (2013). Integrative analysis of complex cancer genomics and clinical profiles using the cBioPortal. *Sci. Signal.* *6*, pii1.

Grassilli, E., Narloch, R., Federzoni, E., Ianzano, L., Pisano, F., Giovannoni, R., Romano, G., Masiero, L., Leone, B.E., Bonin, S., et al. (2013). Inhibition of GSK3B bypass drug resistance of p53-null colon carcinomas by enabling necroptosis in response to chemotherapy. *Clin. Cancer Res.* *19*, 3820–3831.

Gurniak, C.B., and Berg, L.J. (1996). A new member of the Eph family of receptors that lacks protein tyrosine kinase activity. *Oncogene* *13*, 777–786.

Helal, G.K., and Helal, O.K. (2009). Metallothionein attenuates carmustine-induced oxidative stress and protects against pulmonary fibrosis in rats. *Arch. Toxicol.* *83*, 87–94.

Helleday, T., Petermann, E., Lundin, C., Hodgson, B., and Sharma, R.A. (2008). DNA repair pathways as targets for cancer therapy. *Nat. Rev. Cancer* *8*, 193–204.

Hiom, K. (2005). DNA repair: how to PIKK a partner. *Curr. Biol.* *15*, R473–R475.

Hirose, Y., Berger, M.S., and Pieper, R.O. (2001). p53 effects both the duration of G2/M arrest and the fate of temozolomide-treated human glioblastoma cells. *Cancer Res.* *61*, 1957–1963.

Hoadley, K.A., Yau, C., Hinoue, T., Wolf, D.M., Lazar, A.J., Drill, E., Shen, R., Taylor, A.M., Cherniack, A.D., Thorsson, V., et al.; Cancer Genome Atlas Network (2018). Cell-of-origin patterns dominate the molecular classification of 10,000 tumors from 33 types of cancer. *Cell* *173*, 291–304.e6.

Jackson, S.P., and Bartek, J. (2009). The DNA-damage response in human biology and disease. *Nature* *461*, 1071–1078.

Johannessen, C.M., Boehm, J.S., Kim, S.Y., Thomas, S.R., Wardwell, L., Johnson, L.A., Emery, C.M., Stransky, N., Cogdill, A.P., Barretina, J., et al. (2010). COT drives resistance to RAF inhibition through MAP kinase pathway reactivation. *Nature* *468*, 968–972.

- Kandpal, R.P. (2010). Tyrosine kinase-deficient EphB6 receptor-dependent alterations in proteomic profiles of invasive breast carcinoma cells as determined by difference gel electrophoresis. *Cancer Genomics Proteomics* 7, 253–260.
- Kharbanda, S., Yuan, Z.M., Weichselbaum, R., and Kufe, D. (1998). Determination of cell fate by c-Abl activation in the response to DNA damage. *Oncogene* 17, 3309–3318.
- Klaeger, S., Heinzlmeir, S., Wilhelm, M., Polzer, H., Vick, B., Koenig, P.-A., Reinecke, M., Ruprecht, B., Petzoldt, S., Meng, C., et al. (2017). The target landscape of clinical kinase drugs. *Science* 358, eaan4368.
- Kondo, N., Takahashi, A., Ono, K., and Ohnishi, T. (2010). DNA damage induced by alkylating agents and repair pathways. *J. Nucleic Acids* 2010, 543531–543537.
- Kuleshov, M.V., Jones, M.R., Rouillard, A.D., Fernandez, N.F., Duan, Q., Wang, Z., Koplev, S., Jenkins, S.L., Jagodnik, K.M., Lachmann, A., et al. (2016). Enrichr: a comprehensive gene set enrichment analysis web server 2016 update. *Nucleic Acids Res.* 44 (W1), W90–W97.
- Kusebauch, U., Campbell, D.S., Deutsch, E.W., Chu, C.S., Spicer, D.A., Bruniak, M.-Y., Slagel, J., Sun, Z., Stevens, J., Grimes, B., et al. (2016). Human SRMATlas: A Resource of Targeted Assays to Quantify the Complete Human Proteome. *Cell* 166, 766–778.
- Lazzaro, F., Giannattasio, M., Puddu, F., Granata, M., Pelliccioli, A., Plevani, P., and Muzi-Falconi, M. (2009). Checkpoint mechanisms at the intersection between DNA damage and repair. *DNA Repair (Amst.)* 8, 1055–1067.
- Le, Q., Yao, W., Chen, Y., Yan, B., Liu, C., Yuan, M., Zhou, Y., and Ma, L. (2016). GRK6 regulates ROS response and maintains hematopoietic stem cell self-renewal. *Cell Death Dis.* 7, e2478.
- Lee, K.K., Ohyama, T., Yajima, N., Tsubuki, S., and Yonehara, S. (2001). MST, a physiological caspase substrate, highly sensitizes apoptosis both upstream and downstream of caspase activation. *J. Biol. Chem.* 276, 19276–19285.
- Lin, C.-P., Ban, Y., Lyu, Y.L., and Liu, L.F. (2009). Proteasome-dependent processing of topoisomerase I-DNA adducts into DNA double strand breaks at arrested replication forks. *J. Biol. Chem.* 284, 28084–28092.
- Mahajan, K., Coppola, D., Rawal, B., Chen, Y.A., Lawrence, H.R., Engelman, R.W., Lawrence, N.J., and Mahajan, N.P. (2012). Ack1-mediated androgen receptor phosphorylation modulates radiation resistance in castration-resistant prostate cancer. *J. Biol. Chem.* 287, 22112–22122.
- Malumbres, M. (2014). Cyclin-dependent kinases. *Genome Biol.* 15, 122.
- Manic, G., Obrist, F., Sistigu, A., and Vitale, I. (2015). Trial watch: targeting ATM-CHK2 and ATR-CHK1 pathways for anticancer therapy. *Mol. Cell. Oncol.* 2, e1012976.
- Manning, G., Whyte, D.B., Martinez, R., Hunter, T., and Sudarsanam, S. (2002). The protein kinase complement of the human genome. *Science* 298, 1912–1934.
- Maréchal, A., and Zou, L. (2013). DNA damage sensing by the ATM and ATR kinases. *Cold Spring Harb. Perspect. Biol.* 5, a012716.
- Meng, Z., Capalbo, L., Glover, D.M., and Dunphy, W.G. (2011). Role for casein kinase 1 in the phosphorylation of Claspin on critical residues necessary for the activation of Chk1. *Mol. Biol. Cell* 22, 2834–2847.
- Muellner, M.K., Duernberger, G., Ganglberger, F., Kerzendorfer, C., Uras, I.Z., Schoenegger, A., Bagienski, K., Colinge, J., and Nijman, S.M.B. (2014). TOPS: a versatile software tool for statistical analysis and visualization of combinatorial gene-gene and gene-drug interaction screens. *BMC Bioinformatics* 15, 98.
- Muniandy, P.A., Liu, J., Majumdar, A., Liu, S.-T., and Seidman, M.M. (2010). DNA interstrand crosslink repair in mammalian cells: step by step. *Crit. Rev. Biochem. Mol. Biol.* 45, 23–49.
- Nikolova, T., Roos, W.P., Krämer, O.H., Strik, H.M., and Kaina, B. (2017). Chloroethylating nitrosoureas in cancer therapy: DNA damage, repair and cell death signaling. *Biochim. Biophys. Acta Rev. Cancer* 1868, 29–39.
- Pujol-Carrion, N., and de la Torre-Ruiz, M.A. (2010). Glutaredoxins Grx4 and Grx3 of *Saccharomyces cerevisiae* play a role in actin dynamics through their Trx domains, which contributes to oxidative stress resistance. *Appl. Environ. Microbiol.* 76, 7826–7835.
- Resnik, P. (1999). Semantic similarity in a taxonomy: an information-based measure and its application to problems of ambiguity in natural language. *J. Artif. Intell. Res* 11, 95–130.
- Rogakou, E.P., Nieves-Neira, W., Boon, C., Pommier, Y., and Bonner, W.M. (2000). Initiation of DNA fragmentation during apoptosis induces phosphorylation of H2AX histone at serine 139. *J. Biol. Chem.* 275, 9390–9395.
- Rousseeuw, P.J. (1987). Silhouettes: a graphical aid to the interpretation and validation of cluster analysis. *J. Comput. Appl. Math.* 20, 53–65.
- Shafman, T., Khanna, K.K., Kedar, P., Spring, K., Kozlov, S., Yen, T., Hobson, K., Gatei, M., Zhang, N., Watters, D., et al. (1997). Interaction between ATM protein and c-Abl in response to DNA damage. *Nature* 387, 520–523.
- Shrivastav, M., De Haro, L.P., and Nickoloff, J.A. (2008). Regulation of DNA double-strand break repair pathway choice. *Cell Res.* 18, 134–147.
- Smyth, G.K. (2004). Linear models and empirical bayes methods for assessing differential expression in microarray experiments. *Stat. Appl. Genet. Mol. Biol.* 3, Article3.
- Supek, F., Bošnjak, M., Škunca, N., and Šmuc, T. (2011). REVIGO summarizes and visualizes long lists of gene ontology terms. *PLoS ONE* 6, e21800.
- Suzuki, A., Hirata, M., Kamimura, K., Maniwa, R., Yamanaka, T., Mizuno, K., Kishikawa, M., Hirose, H., Amano, Y., Izumi, N., et al. (2004). aPKC acts upstream of PAR-1b in both the establishment and maintenance of mammalian epithelial polarity. *Curr. Biol.* 14, 1425–1435.
- Thomas, A., Tanaka, M., Trepel, J., Reinhold, W.C., Rajapakse, V.N., and Pommier, Y. (2017). Temozolomide in the era of precision medicine. *Cancer Res.* 77, 823–826.
- Torkamani, A., Verkhivker, G., and Schork, N.J. (2009). Cancer driver mutations in protein kinase genes. *Cancer Lett.* 281, 117–127.
- Viniegra, J.G., Martínez, N., Modirassari, P., Hernández Losa, J., Parada Cobo, C., Sánchez-Arévalo Lobo, V.J., Aceves Luquero, C.I., Alvarez-Vallina, L., Ramón y Cajal, S., Rojas, J.M., and Sánchez-Prieto, R. (2005). Full activation of PKB/Akt in response to insulin or ionizing radiation is mediated through ATM. *J. Biol. Chem.* 280, 4029–4036.
- Vinjamuri, M., Adumala, R.R., Altaha, R., Hobbs, G.R., and Crowell, E.B., Jr. (2009). Comparative analysis of temozolomide (TMZ) versus 1,3-bis(2-chloroethyl)-1 nitrosourea (BCNU) in newly diagnosed glioblastoma multiforme (GBM) patients. *J. Neurooncol.* 91, 221–225.
- Wang, Y., Yang, F., Gritsenko, M.A., Wang, Y., Claus, T., Liu, T., Shen, Y., Monroe, M.E., Lopez-Ferrer, D., Reno, T., et al. (2011). Reversed-phase chromatography with multiple fraction concatenation strategy for proteome profiling of human MCF10A cells. *Proteomics* 11, 2019–2026.
- William-Faltaos, S., Rouillard, D., Lechat, P., and Bastian, G. (2007). Cell cycle arrest by oxaliplatin in cancer cells. *Fundam. Clin. Pharmacol.* 21, 165–172.
- Wiśniewski, J.R., Zougman, A., Nagaraj, N., and Mann, M. (2009). Universal sample preparation method for proteome analysis. *Nat. Methods* 6, 359–362.
- Xu, L.-Q., Tan, S.-B., Huang, S., Ding, H.-Y., Li, W.-G., Zhang, Y., Li, S.-Q., and Wang, T. (2017). G protein-coupled receptor kinase 6 is overexpressed in glioma and promotes glioma cell proliferation. *Oncotarget* 8, 54227–54235.
- Zirkin, S., Davidovich, A., and Don, J. (2013). The PIM-2 kinase is an essential component of the ultraviolet damage response that acts upstream of E2F-1 and ATM. *J. Biol. Chem.* 288, 21770–21783.

STAR★METHODS

KEY RESOURCES TABLE

REAGENT or RESOURCE	SOURCE	IDENTIFIER
Antibodies		
Mouse monoclonal anti-phospho-H2A.X (Ser139), γ -H2AX, clone JBW301	Merck	Cat#05-636; RRID:AB_309864
Alexa Fluor® 647 conjugate, goat anti-Mouse IgG (H+L)	Thermo Fisher Scientific	Cat#A-21235; RRID:AB_2535804
Rabbit Anti-HA tag antibody - ChIP Grade	Abcam	Cat#ab9110; RRID:AB_307019
Rabbit MARK3 antibody	Cell Signaling	Cat#9311, RRID:AB_2297393
Goat Anti-Rabbit IgG, HRP-linked Antibody	Cell Signaling	Cat#7074, RRID:AB_2099233
Bacterial and Virus Strains		
Subcloning Efficiency DH5alpha Competent Cells	Thermo Fisher	Cat# 18265017
Chemicals, Peptides, and Recombinant Proteins		
5-Aza-2'-Deoxycytidine (Decitabine)	Sigma-Aldrich	Cat#A3656
Aphidicolin from Nigrospora sphaerica	Sigma-Aldrich	Cat#A0781
Camptothecin	Sigma-Aldrich	Cat#C9911
Carmustine	Sigma-Aldrich	Cat#C0400
Cytarabine	Sigma-Aldrich	Cat#PHR1787
Doxorubicin	Sigma-Aldrich	Cat#D1515
Etoposide	Sigma-Aldrich	Cat#E1383
Hydroxyurea	Sigma-Aldrich	Cat#H8627
Topotecan	Sigma-Aldrich	Cat#T2705
UCN-01	Sigma-Aldrich	Cat#U6508
Oxaliplatin	Sigma-Aldrich	Cat#O9512
Temozolomide	Sigma-Aldrich	Cat#T2577
Critical Commercial Assays		
Click-iT EdU Alexa Fluor 488 Flow Cytometry Assay Kit	Thermo Fisher Scientific	Cat#C10420
CellTiter-Glo® Luminescent Cell Viability Assay	Promega	Cat#G7570
<i>In Situ</i> Cell Death Detection Kit TMR red	Sigma-Aldrich	Cat#12156792910
DAPI	Sigma-Aldrich	Cat#D9542
Pierce BCA Protein Assay Kit	Thermo Fisher Scientific	Cat#23225
Experimental Models: Cell Lines		
HAP1 wild type	Horizon Genomics	Cat#C859
HAP1 kinome knockout collection	Horizon Genomics	https://www.horizondiscovery.com/catalog/search/result?q=kinase
HEK293T	CR-UK	N/A
RPE1	CR-UK	N/A
Oligonucleotides		
MARK3 gRNA1, 5'-AGTCTGTAGTTTCCGATGTG-3'	Sigma-Aldrich	N/A
MARK3 gRNA2, 5'-AGTGATCTCAACAACAGTAC-3'	Sigma-Aldrich	N/A
Non-target gRNA, 5'-TACGCGAGATCGTTCCGGTC-3'	Sigma-Aldrich	N/A
Recombinant DNA		
pDONR223 for kinases	Addgene	https://www.addgene.org/browse/article/3878/
pLIX_402	Addgene	Cat#41394
CMV-GFP	CeMM	N/A
VSV-G	CeMM	N/A
dR8.91	CeMM	N/A
PLCV2	Addgene	Cat#52961; RRID:Addgene_52961

(Continued on next page)

Continued		
REAGENT or RESOURCE	SOURCE	IDENTIFIER
Software and Algorithms		
BLASTN	Altschul et al., 1990	https://blast.ncbi.nlm.nih.gov/Blast.cgi ; RRID:SCR_001598
TOPS	Muellner et al., 2014	https://sourceforge.net/p/topscemm/wiki/Home/
FlowJo	FlowJo Software	https://www.flowjo.com/ ; RRID:SCR_008520
R project	The R Project for Statistical Computing	https://www.r-project.org/ ; RRID:SCR_001905
Enrichr	Chen et al., 2013; Kuleshov et al., 2016	http://amp.pharm.mssm.edu/Enrichr/ ; RRID:SCR_001575
Revigo	Supek et al., 2011	http://revigo.irb.hr/ ; RRID:SCR_005825
cBioPortal	Gao et al., 2013; Cerami et al., 2012	http://www.cbioportal.org/ ; RRID:SCR_014555
SRM atlas	Kusebauch et al., 2016	http://www.mrmatlas.org/
LIMMA	Benjamini and Hochberg, 2018	http://bioinf.wehi.edu.au/limma/ ; RRID:SCR_010943
Other		
BD LSRFortessa cell analyzer	BD Biosciences	N/A
Echo 520	Labcyte	N/A
Covaris S2 high performance ultrasonicator	Covaris	N/A
Orbitrap Fusion Lumos mass spectrometer	Thermo Fisher Scientific	N/A

CONTACT FOR REAGENT AND RESOURCE SHARING

Further information and requests for resources and reagents should be directed to and will be fulfilled by the Lead Contact, Joanna Loizou (jloizou@cemm.oeaw.ac.at).

EXPERIMENTAL AND SUBJECT DETAILS

Cell Lines

HAP1 knockout cell lines were generated using CRISPR-Cas9 gene editing technology in collaboration with Horizon Genomics (Vienna Austria) as single clones. They were grown in Iscove's Modified Dulbecco's Medium (IMDM) from GIBCO®, containing L-Glutamine and 25 mM HEPES and supplemented with 10% heat-inactivated fetal bovine serum (FBS) and 1% penicillin-streptomycin (P/S at 100µg/mL) and passaged according to standard protocol with trypsin and PBS. All cell lines were grown at 37°C in a 3% oxygen and 5% CO₂-humidified incubator.

HEK293T cells used for virus production were expanded in Dulbecco's Modified Eagle Medium (DMEM), supplemented with 10% FBS and 1% P/S. Cells were grown at 37°C in a 3% oxygen and 5% CO₂ incubator.

RPE1 cells were cultured in in DMEM:F12 supplemented with 10% FBS and 1% P/S. Cells were grown at 37°C in a 3% oxygen and 5% CO₂ incubator.

METHOD DETAILS

Confirmation of CRISPR-Cas9 Targeting by Sanger Sequencing

HAP1 kinase deficient knockout cell lines were validated for gene editing leading to a frameshift mutation in the respective genes. We designed forward and reverse primers for each gene and purchased oligonucleotides from Sigma-Aldrich (Sequences can be obtained at <https://www.horizondiscovery.com/>). For genomic DNA extraction, cells were treated with trypsin and washed twice with PBS, then resuspended in 100µL Direct PCR-Cell lysis solution with 2µL Proteinase K (20mg/mL). Wells were sealed and heated for 2.5 hours at 56°C, then 45 minutes at 80°C to inactivate Proteinase K, followed by PCR amplification. PCR amplification conditions: heat lid 110°C; 94°C 2 minutes; loop 35x (94°C 30 s; 337 55°C 30 s; 68°C 1 minute) 68°C 7 minutes. Then the PCR product was purified using Rapid PCR Cleanup Enzyme Set from BioLabs Inc., diluted 1:2 with double distilled water (ddH₂O) and sequenced by Microsynth AG. Results were aligned to respective genes using Basic Local Alignment Search Tool, BLAST provided by NCBI.

High-throughput Drug Screen

Indicated volumes and concentrations of compounds (Table S5) per well were transferred into 384-well plates (Corning 3712) from DMSO stock plates using acoustic transfer (Labcyte Echo 520). Wild-type or knockout HAP1 cells (at an amount of 1,000 cells) were seeded in 50 μ L media into the compound-containing plates. Three days later cell viability was determined using Cell Titer-Glo (Promega). Compounds were used at 4 dose points with 4 replicates.

FACS Screen

Cell Culture

HAP1 cells were cultured as described above for 7 days until 80%–90% confluence. Every HAP1 cell line was seeded into 4 Costar® 6-well cell culture plates, each plate at a density (cell number/well) according to the time-points of harvest: 160,000 for 5-hours treatment, 80,000 for 24 hours treatment, 20,000 for 24 hours post treatment and 10,000 for 48 hours post treatment.

Drug treatment

The day after seeding, cells were treated with 6 concentrations of the respective compound. The highest concentration- temozolomide, 250 μ M; oxaliplatin, 780 nM- was chosen to moderately affect wild-type cells (10 - 30% cell death). The compounds were serially diluted 1:2 from the highest to lowest dose. For the untreated control we used DMSO at a concentration corresponding to the lowest compound dilution. After 24 hours treatment, media from the remaining time points was aspirated and replaced with 2 mL of fresh (drug-free) IMDM medium. 40 minutes before each harvest 5-ethynyl-2'-deoxyuridine (EdU) at a concentration of 10 μ M was added to each well.

Cell harvest

Cells were washed with 400 μ L phosphate buffer saline (PBS) and detached with 500 μ L trypsin, collected with 1 mL of medium, transferred into 96-deep-well (2ml) plates and centrifuged at 2,000 rpm for 6 min. The supernatant was carefully discarded, cell pellets were washed with PBS and re-suspended in 100 μ L fixing solution, containing 4% para-formaldehyde (PFA) and 0.1% Triton X, transferred into V-bottom shaped 96-well plates, incubated at 4°C and then stained.

FACS staining

96-well plates, containing fixed cells, were centrifuged at 1,200 rpm for 6 min then washed with 50 μ L PBS. Pellets were re-suspended in TUNEL staining solution (*In Situ* Cell Death Detection Kit, TMR red, Sigma Aldrich) containing anti-phospho-H2A.X (Ser139) i.e., γ H2AX, clone JBW301 (1:500 dilution, MILLIPORE) and incubated for one hour in the dark at 37°C. Then the pellets were washed three times with PBS (with centrifugations at 1,200 rpm for 6 min) and re-suspended with Click-iT EdU Alexa Fluor 488 Flow Cytometry Assay Kit staining solution (Thermo Fisher Scientific) containing secondary antibody (1:500 dilution, Alexa Fluor® 647 conjugate, goat anti-Mouse IgG (H+L), Thermo Fisher Scientific) for detection of γ H2AX and incubated for one hour in the dark at room temperature (RT). Subsequently pellets were washed three times with PBS and re-suspended in DAPI (Sigma Aldrich) solution (1:1,000 dilution) and kept dark. Samples were measured using the BD LSRFortessa cell analyzer machine.

Reconstitution of Knockout Cell Lines

For reconstitution of the respective wild-type genes in knockout cell lines, we used Gateway- cloning compatible vector backbones containing the gene of interest and a spectinomycin resistance cassette, from Addgene. These plasmids of the kind "pDONR223-XXX" were a gift from William Hahn & David Root (Johannessen et al., 2010). Bacterial DH5 α were grown on agar plates containing spectinomycin, from which a single clone was picked and cultured in LB-media containing spectinomycin overnight at 37°C. Plasmids were purified using Quiagen MidiPrep Kit and the LR-reaction was performed according to the Gateway Technology protocol provided by Invitrogen. We transferred the cDNA of the gene of interest into the doxycycline inducible pLIX_402 entry vector for mammalian expression and lentivirus production containing an Amp^R cassette. The entry clones were transformed into Mg²⁺/Ca²⁺ competent DH5 α strains, amplified in an overnight culture in LB-media containing ampicillin and plasmids were extracted using QIAGEN MidiPrep Kit. Lentivirus particles were produced using following plasmids: CMV-GFP, VSV-G and dR8.91. Virus was harvested for two days in the mornings and evenings. Knockout cells were infected with virus particles containing the respective gene, selected for 2 days with puromycin at 2 μ g/mL and cells were propagated for another 2 days.

Survival Dose Responses

Dose response curves for temozolomide, oxaliplatin, hydroxyurea and doxorubicin were generated by seeding cells in 96-well plates (1,000 cells/well). The next day, compounds were added at the indicated concentrations. Cells harboring the reconstituted gene of interest were additionally treated with doxycycline at 1 μ g/mL every day. Three days after drug treatment, cell viability was measured using the CellTiter-Glo assay protocol (Promega).

Immunoblotting and Antibodies

Cells were harvested and then lysed with RIPA lysis buffer (NEB) supplemented with protease and phosphatase inhibitors from Sigma. Western blots were performed according to standard protocols. Protein samples were separated using NuPAGE 4%–12% gradient Bis-Tris Protein Gels from Invitrogen and MOPS running buffer at 120 V for 2 hours running time. The separated proteins were then transferred onto nitrocellulose membranes. To prevent unspecific protein binding, membranes were treated with blocking solution (5% milk in TBST) for 1 hour and primary antibodies were added at 1:1,000 to the blocking solution and

incubated overnight at 4°C. The next day, membranes were washed 3x with TBST and incubated with secondary antibodies at 1:5,000 in 5% milk/TBST solution. Then membranes were treated with immunoblotting developer solution (GSE) for 1 minute and imaged in the dark. The following antibodies were used: primary; Rabbit Anti-HA tag antibody - ChIP Grade (ab91110, Abcam), MARK3 (9311, Cell Signaling), secondary; Goat Anti-Rabbit IgG, HRP-linked Antibody (#7074, Cell Signaling).

Targeting of MARK3 by CRISPR-Cas9 in RPE1 cells

RPE1 cells lacking MARK3 were generated using the gRNA used in HAP1 (5'-AGTCTGTAGTTTCCGATGTG-3') and a second non-overlapping gRNA (5'-AGTGATCTCAACAACAGTAC-3'). A non-targeting gRNA (5'-TACGCGAGATCGTTCCGGTC-3') was used as a control. The gRNAs were cloned into PLCV2 vectors and transformed into HEK293T cells for virus production. RPE1 cells were infected with the virus and following selection with puromycin for 2 days, were used for survival and immunoblot.

Phosphoproteomics

Drug treatment

MARK3 knockout or wild-type HAP1 cells were treated with 62.5 μ M TMZ for 24 hours. Cells were harvested and cell pellets were frozen with liquid nitrogen and kept at -80°C .

Sample preparation and phosphopeptide enrichment

Each washed cell pellet was lysed separately in 40 μ L of freshly prepared lysis buffer containing 50 mM HEPES (pH 8.0), 2% SDS, 0.1 M DTT, 1 mM PMSF, phosSTOP and protease inhibitor cocktail (Sigma-Aldrich). Samples rested at room temperature (RT) for 20 min before heating to 99°C for 5 min. After cooling down to RT, DNA was sheared by sonication using a Covaris S2 high performance ultrasonicator. Cell debris was removed by centrifugation at 20,000 \times g for 15 min at 20°C. Supernatant was transferred to fresh eppendorf tubes and protein concentration determined using the BCA protein assay kit (Pierce Biotechnology, Rockford, IL). FASP was performed using a 30 kDa molecular weight cutoff filter (VIVACON 500; Sartorius Stedim Biotech GmbH, 37070 Goettingen, Germany) essentially according to the procedure described (Wiśniewski et al., 2009). In brief, 100 μ g total protein per sample were reduced by adding DTT at a final concentration of 83.3 mM followed by incubation at 99°C for 5 min. After cooling to RT, samples were mixed with 200 μ L of freshly prepared 8 M urea in 100 mM Tris-HCl (pH 8.5) (UA-solution) in the filter unit and centrifuged at 14,000 \times g for 15 min at 20°C to remove SDS. Any residual SDS was washed out by a second washing step with 200 μ L of UA. The proteins were alkylated with 100 μ L of 50 mM iodoacetamide in the dark for 30 min at RT. Afterward, three washing steps with 100 μ L of UA solution were performed, followed by three washing steps with 100 μ L of 50 mM TEAB buffer (Sigma-Aldrich). Proteins were digested with trypsin at a ratio of 1:50 overnight at 37°C. Peptides were recovered using 40 μ L of 50 mM TEAB buffer followed by 50 μ L of 0.5 M NaCl (Sigma-Aldrich). Peptides were desalted using C18 solid phase extraction spin columns (The Nest Group, Southborough, MA). After desalting, peptides were labeled with TMT 11plex reagents according to the manufacturer (Pierce, Rockford, IL). After quenching of the labeling reaction, labeled peptides were pooled, organic solvent removed in vacuum concentrator and labeled peptides cleaned via C18 solid phase extraction (SPE). Peptides were eluted with 80% acetonitrile containing 0.1% trifluoroacetic at a final peptide concentration of $\sim 1\mu\text{g}/\mu\text{L}$. Eluate was then used for phosphopeptide enrichment applying a modified method of immobilized metal affinity chromatography (IMAC). Briefly, three times 100 μ L of Ni-NTA superflow slurry (QIAGEN Inc., Valencia, USA) were washed with LCMS-grade water and Ni²⁺ stripped off the beads by incubation with 100 mM of EDTA, pH 8 solution for 1 hour at room temperature. Stripped NTA resin was recharged with Fe³⁺-ions by incubation with a fresh solution of Fe(III)Cl₃ and 100 μ L of charged resin slurry used for the enrichment of a total of $\sim 400\mu\text{g}$ TMT-labeled peptides. The unbound fraction was transferred to a fresh glass vial and used for offline fractionation for the analysis of the whole proteome. After washing the slurry with 0.1% TFA, phosphopeptides were eluted with a freshly prepared ammonia solution containing 3mM EDTA, pH 8 and all used for offline fractionation for the analysis of the phosphoproteome.

Offline Fractionation via RP-HPLC at high pH

Tryptic peptides were re-buffered in 20 mM ammonium formate buffer pH 10, shortly before separation by reversed phase liquid chromatography at pH 10. The unbound fraction of the phosphopeptide enrichment was separated into 96 time-based fractions on a Phenomenex column (150 \times 2.0 mm Gemini-NX 3 μ m C18 110Å, Phenomenex, Torrance, CA, USA) using an Agilent 1200 series HPLC system fitted with a binary pump delivering solvent at 100 μ L/min. Acidified fractions were consolidated into 36 fractions via a concatenated strategy described here (Wang et al., 2011). The bound fraction containing the phosphopeptides was separated into 20 fractions on a Dionex column (500 μ m \times 50 mm PepSwift RP, monolithic, Dionex Corporation, Sunnyvale, CA, USA) using an Agilent 1200 series nanopump delivering solvent at 4 μ L/min. Peptides were separated by applying a gradient of 90% acetonitrile containing 20 mM ammonium formate and pH 10. After solvent removal in a vacuum concentrator, samples were reconstituted in 5% formic acid for LC-MS/MS analysis and kept at -80°C until analysis.

2D-RP/RP Liquid Chromatography Mass Spectrometry

Mass spectrometry was performed on an Orbitrap Fusion Lumos mass spectrometer (ThermoFisher Scientific, San Jose, CA) coupled to an Dionex Ultimate 3000RSLC nano system (ThermoFisher Scientific, San Jose, CA) via nanoflex source interface. Tryptic peptides were loaded onto a trap column (Pepmap 100 5 μ m, 5 \times 0.3 mm, ThermoFisher Scientific, San Jose, CA) at a flow rate of 10 μ L/min using 2% ACN and 0.1% TFA as loading buffer. After loading, the trap column was switched in-line with a 30 cm, 75 μ m inner diameter analytical column (packed in-house with ReproSil-Pur 120 C18-AQ, 3 μ m, Dr. Maisch, Ammerbuch-Entringen, Germany). Mobile-phase A consisted of 0.4% formic acid in water and mobile-phase B of 0.4% formic acid in a mix of 90%

acetonitrile and 10% water. The flow rate was set to 230 nL/min and a 90 min gradient used (6 to 30% solvent B within 81 min, 30 to 65% solvent B within 8 min and, 65 to 100% solvent B within 1 min, 100% solvent B for 6 min before equilibrating at 6% solvent B for 18 min). Analysis was performed in a data-dependent acquisition mode. Full MS scans were acquired with a scan range of 375 - 1650 m/z in the orbitrap at a resolution of 120,000 (at 200Th). Automatic gain control (AGC) was set to a target of 2×10^5 and a maximum injection time of 50 ms. Precursor ions for MS² analysis were selected using a TopN dependant scan approach with a max cycle time of 3 s. For improved detection of EPHB6, MARK3, DYRK4, PNCK, NPAT, DNA topoisomerase 2-beta and DNA topoisomerase 2-binding protein 1, an inclusion list for preferential precursor selection was employed for the global proteome analysis. In total, 55 peptide m/z values derived from the SRM atlas (<http://www.mrmatlas.org/>) were specified. MS² spectra were acquired in the orbitrap (FT) at a resolution of 50,000 (at 200 Th). Precursor isolation in the quadrupole was set to 0.7 Da and 1.0 Da for the proteome and phosphoproteome, respectively. Higher energy collision induced dissociation (HCD) was used with a normalized collision energy (NCE) of 38%. AGC was set to 5×10^4 with a maximum injection time of 105 ms and 150 ms for the proteome and phosphoproteome, respectively. Dynamic exclusion for selected ions was 60 s for the proteome and 30 s for the phosphoproteome. A single lock mass at m/z 445.120024 for recalibration was employed. Xcalibur version 4.0.0 and Tune 2.1 were used to operate the instrument.

QUANTIFICATION AND STATISTICAL ANALYSIS

Analysis of high-throughput Drug Screen (Figures 1 and S1, Table S1)

For data analysis, the percentage of control was calculated and the signal of the DMSO treated sample was used to set values to 100% survival, while the 25X camptothecin (cytotoxic concentrations) signal was used to set the values to 0%. Survival circo plot with DNA repair deficient cells (Figure S1) was created using TOPS (Muellner et al., 2014) for analysis and basic visualization. For kinome survival to DNA damage (Figure 1, Table S1), areas under the curve (AUC) were calculated as a cumulative measure of compound potency by taking the sum of the mean of subsequent concentration points (as applied previously (Englinger et al., 2016)).

Clustering Analysis (Figure 1 and Table S1)

Cell lines were clustered with agglomerative clustering using the R package ConsensusClusterPlus. Cell lines and compounds were randomly sub-sampled for 10,000 times and clustered using complete linkage to increase the robustness of clustering. The distance was calculated using the Pearson correlation. The optimal number of clusters (n = 3) was assessed using the silhouette analysis (Rousseeuw, 1987).

GO Term Enrichment Analysis (Figures 1, 4, S1, and S4, Table S1)

GO term enrichments were calculated using Enricher, a comprehensive tool for gene set enrichment analysis (Kuleshov et al., 2016). P values were calculated using a Fisher's exact test and corrected for multiple hypotheses using a cut-off of p value < 0.05. In order to filter for redundant and unspecific GO terms, we first removed all GO terms that are annotated to more than 70 genes and further summarized terms based on their Resnik semantic similarity (Resnik, 1999) using the tool ReviGO (Supek et al., 2011).

FACS Analysis (Figures 2 and S2, Table S2)

For analysis, dead cells were discarded using forward and side scatter and next single cell populations were gated using DAPI width and DAPI area following the Abcam PI staining protocol. Gates for γ H2AX and TUNEL were set for all concentrations according to the untreated (DMSO) control. For all time points, to take all drug concentrations into account, an area-under-the-curve (AUC) of all six dose points was calculated and compared to untreated controls. This data is visualized in the phenotypic FACS plot. The cell cycle phases were determined by gating G1- and G2-phase as well as S-phase of diploid populations using a DAPI against EdU plot. Proliferating cells were determined by setting a threshold for cells with positive EdU incorporation and EdU positive signals were plotted against untreated control cells. Data was analyzed using FlowJo v10.3 and The R Project for Statistical Computing.

Gene Alteration Frequencies (Figure 3)

Gene alteration frequencies were calculated using the TCGA PanCancer dataset (Hoadley et al., 2018) that includes 10967 samples across 33 different tumor types. The data was accessed via the cbiportal webservice (Gao et al., 2013) and frequencies calculated by dividing the amount of samples containing a mutation or deletion within one of the four genes of interest by the total number of samples for a given cancer type.

Analysis of Phosphoproteomics (Figures 4 and S4, Tables S3 and S4)

Acquired raw data files were processed using the Proteome Discoverer 2.2.0. platform, utilizing the Sequest HT database search engine and Percolator validation software node (V3.04) to remove false positives with a false discovery rate (FDR) of 1% on PSM and protein level under strict conditions. Searches were performed with full tryptic digestion against the human SwissProt database v2017.12 (42356 sequences and appended known contaminants) with up to two miscleavage sites. Oxidation (+15.9949 Da) of methionine was set as variable modification, while carbamidomethylation (+57.0214 Da) of cysteine residues and TMT 6-plex

labeling of peptide N-termini and lysine residues were set as fixed modifications. For phosphopeptides phosphorylation (+79.9663 Da) of serine, threonine and tyrosine was additionally included as a variable modification. Data was searched with mass tolerances of ± 10 ppm and 0.025 Da on the precursor and fragment ions (HCD), respectively. Results were filtered to include peptide spectrum matches (PSMs) with Sequest HT cross-correlation factor (Xcorr) scores of ≥ 1 and 1% FDR peptide confidence. The ptmRS algorithm was additionally used to validate phosphopeptides with a set score cutoff of 75. PSMs with precursor isolation interference values of $\geq 50\%$ or average TMT-reporter ion signal-to-noise values (S/N) ≤ 10 were excluded from quantitation. Isotopic impurity correction and TMT channel-normalization based on total peptide amount were applied. TMT channel assignment was as follows: 126: MARK3-KO-1, 127N:MARK3-WT-1, 127C:MARK3-KO-2, 128N:MARK3-WT-2, 128C:MARK3-KO-3, 129N:MARK3-WT-3, 129C:MARK3-KO+DNA damage-1, 130N:MARK3-WT+DNA damage-1, 130C:MARK3-KO+DNA damage-2, 131N:MARK3-WT+DNA damage-2, 131C:MARK3-KO+DNA damage-3. Reporter channel abundances were normalized to equal total peptide signal in each TMT channel. The phosphoproteomics experiment was acquired in two technical replicates. Phosphopeptides observed only in a single technical replicate or those where the difference between the two technical measurements of any TMT channel was more than 20% of the most intense TMT channel of that phosphopeptide (averaged over the two replicates) were excluded from the further analysis. The arithmetic average of relative intensities (relative against the sum of all 11 reporter channels of the given technical replicate) were used as the final measure of the phosphopeptide abundance changes. As the last normalization step, the phosphopeptide abundances were further normalized for protein abundance changes. LIMMA statistical model (Smyth, 2004) and Benjamini-Hochberg procedure (FDR correction) were used to calculate statistical significance of observed changes on protein and phosphopeptide level. TMT ratios with Q-values lower than 0.01 were considered as significant. The ratio thresholds used in Figures 4 and S4 are $\pm \log_2(1.45)$ and $\pm \log_2(1.15)$ for phosphoproteomics and proteomics respectively. These thresholds corresponded to the 5% quantile of the distribution of ratios observed among biological replicates within the same sample types (e.g., meaning that biologically replicated measurements of protein abundances within the same condition differ from each other by more than $\pm \log_2(1.15)$ only for 5% of quantified proteins).